The Future of Gas Turbine Technology
8th International Gas Turbine Conference
12-13 October 2016, Brussels, Belgium

Paper ID Number (*67-IGTC16)*

GAS TURBINE FLEXIBILITY AND LIFE ASSESSMENT METHOD

David Bosak[1], Siddig Dabbashi, Thank-God Isaiah, Pericles Pilidis, Giuseppina Di-Lorenzo

Cranfield University, Cranfield, Bedfordshire, UK, MK43-0AL
[1] david.bosak@gmail.com

ABSTRACT

In the current European energy market situation, gas power plants are required to operate in cyclical modes to fill the gaps in renewable energy supply. Renewable sources have priority in dispatching due to their relatively low variable operational costs. However, because of their high unpredictability, conventional power plants such as Simple Cycle Power Plants (SCPP) and Combined Cycle Power Plants (CCPP) suffer frequent load changes to fill the gaps in supply by participating in the balancing market. In this paper, the development work of two maps is presented. The first aims to provide a method to quickly assess life consumption in a critical gas path component. The second aims to provide a method to quickly assess gas turbine operational flexibility and performance trade-offs arising from various load change strategies. The results are speculated to support plant operators in load change decision making while exposing potential trade-offs in life consumption and flexible performance.

Keywords: gas turbine, flexibility, performance, life consumption, trade-offs

INTRODUCTION

The realization of dramatic consequences from global warming lead to increasing mothballing of polluting power plants in attempt to reduce global production of green-house emissions. The resulting gap in capacity is filled with increasing mix of renewable/clean power generation. However, the irregular nature of renewable sources presents a challenge to dispatchers to fill comparatively much more stable electricity demand. The Combined Cycle Power Plants (CCPP) and Simple Cycle Power Plants (SCPP) provide a promising solution due to their much better load response characteristics than other conventional power plants such as coal or nuclear. Most of the existing CCPP and SCPP plants were built more than 20 years ago and were not designed to operate in cyclic modes, which now suffer frequent load changes as demanded by the competitive market. Because of more frequent operation at part-load, these power plants now suffer from higher variable operational costs due to lower thermal efficiencies and higher life consumption at part-load.

The variable operating costs of power plants are a key factor in determining which units are dispatched first to meet the demand. Since renewable power plants have nearly negligible variable operating costs and are unpredictable, they have priority in dispatching and any gap in supply when renewable sources are unavailable needs to be filled quickly with other traditional power plants e.g. CCPP or SCPP. The extent to which renewable sources are unpredictable was experienced by Spain, where on the 17 September 2012 wind covered 1% of the instantaneous demand and one week later the production increased to 64% of the instantaneous demand (Alvarez, 2016). It is clear that conventional power plant operators need to look for solutions in order to remain competitive in the current market.

Economic Pressure

A load profile of a particular CCPP power plant in the UK on the 17 February 2016 is shown in Figure 1. The solid line represents the actual contracted load level, and the dotted line represents contracted load level in the balancing market. The balancing mechanism is used to continuously balance the grid to meet the demand by filling in the gaps generated by risky and unpredictable renewable electricity. When participating in the balancing market, the conventional power plant operator, such as the one operating in Figure 1, receives additional income stream by diverging from the original contracted load (solid line). Therefore, being able to provide much faster load response service, or in other words have higher plant flexibility, provides competitive advantage and higher revenue. However, this comes at a cost of increased life consumption of critical plant components and deterioration in thermal efficiency which leads to higher operational costs. Any short-notice load change induces additional thermal and mechanical stresses on the plant components, which effectively consume critical component life and

shift the plant maintenance period closer to the date of execution.

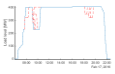

Figure 1 Combined Cycle Power Plant (CCPP) load level profile on 17 February 2016. Dotted line shows load change in the balancing market (Balancing Mechanism Reporting System (BMRS)).

Power plant operators are usually provided by Original Equipment Manufacturers (OEM) with a pre-determined maintenance schedule based on equivalent working hours. This schedule is used to estimate the next plant shut down for maintenance. It is, however, difficult to justify the details and trade-offs on how the maintenance schedule would shift when the operator assesses economic and financial feasibility of participating in the balancing market.

In this paper gas turbine performance and life consumption maps are presented. The aim is provide a robust and simple method to aid assessing life consumption and performance trade-offs of flexible gas turbine operation as required by the current market condition. The power plant operator can use these maps to estimate life consumption, decide on the best load change strategy, and quickly assess trade-offs in performance at the time when decision is made whether to participate in the balancing market.

GAS TURBINE PERFORMANCE SIMULATIONS

Gas turbine part-load performance has been modeled with Cranfield in-house performance modeling program TURBOMATCH. Design point parameters for single and multi-shaft engine are listed in Table 1.

Table 1 Gas turbine design performance parameters

	Single shaft	Multi shaft
Power output	400 MW	32 MW
Engine pressure ratio	19.2	22.8
TET	1680 K	1550 K
Inlet air mass flow	845 kg/s	97 kg/s
Fuel type	Natural gas	Natural gas
Compressor1 efficiency	89%	88%
Compressor2 efficiency	---	88%
Cooling air extraction	10%	5%
Turbine1 efficiency	91%	89%
Turbine2 efficiency	---	88%
Free power turbine efficiency	---	88%
Combustion efficiency	99%	99%
Combustor pressure loss	5%	5%
Intake pressure loss	0%	0%
Exhaust pressure loss	2%	2%

DEVELOPMENT OF LIFE CONSUMPTION MAP

First stage high pressure turbine rotor blades are critical components for failure analysis. These blades operate in harsh environment with temperatures usually exceeding the alloy melting point temperature. Significant progress over decades in blade cooling technologies allowed for achieving increasingly higher power output, however, at the cost of higher component life consumption.

High pressure turbine blades operating in these conditions are prompt to failure under various mechanisms. The blade will fail under low cycle fatigue leading to fracture if low frequencies of significantly high stress amplitudes induce plastic strains in the material. This is a typical scenario for plant start-stop cycles, or load changes.

On the other hand, the blade will fail under creep deformation leading to fracture under the influence of high temperature and high stress for prolonged periods of time. This is a typical mechanism experienced by high pressure turbine blades when plant is in operation.

In the following calculations it is assumed the blade alloy to be NIMONIC 115, which is a common nickel based alloy used for manufacturing of turbine blades. In order to avoid excessive blade temperature, the cooling air is extracted from a location within the engine of similar pressure but lower temperature to maximise heat transfer. It is a common practice to extract cooling air from the last stage of high pressure compressor, however, at the expense of reduced engine power.

Assuming the blade cooling effectiveness of 0.637 and steady state conditions, the blade temperature is calculated with Equation 1.

Equation 1

$$T_{blade} = TET - CE(TET - T_{cooling})$$

Figure 2 shows simulated variation of TET, $T_{cooling}$, and T_{blade} in the operating range of single shaft and multi shaft gas turbine engine against alloy melting point temperature (Nimonic alloy 115). Since the single shaft engine operates at much higher power, the TET exceeds alloy melting temperature in the high power region and the use of cooling is inevitable.

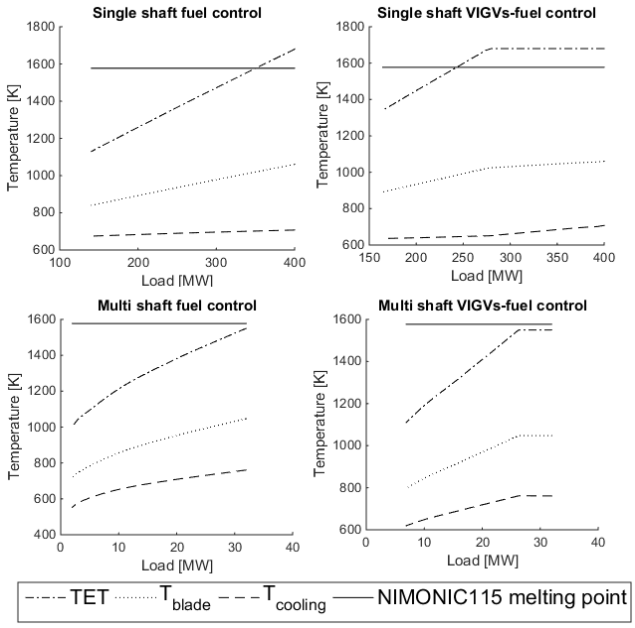

Figure 2 Simulated results of single and multi-shaft gas turbine performance at part-load versus turbine blade melting point temperature.

High pressure turbine blade experiences various forces, with the highest centrifugal force acting at the root of the blade. Other sources of stress include gas bending moment due to changes in gas momentum and pressure across the blade, gas bending moment due to centrifugal loading if blade centre of mass doesn't align radially above the centroid of the disc, stress due to thermal gradients across the blade, and sometimes vibrations arising from acoustic oscillations in the combustor.

In the following calculations only centrifugal stress is taken into account, which is calculated with Equation 2.

Equation 2

$$Centrifugal\ stress = \frac{\rho\omega^2}{2}\left({R_t}^2 - {R_r}^2\right)$$

The blade root and tip radius is assumed to be 0.81m and 0.89m, respectively. Any geometric modifications to the blade create local regions of stress concentration. These are usually at the blade root to provide adequate mounting, and sealing methods. In the following calculations, it was assumed that stress concentration factor at the root of the blade is $K_t = 2.82$. Because of the inevitable existence of local region of stress concentration, the region should be carefully examined against failure. This has lead to the development of robust and simple fatigue and creep life consumption maps.

LOW CYCLE FATIGUE FAILURE IN HIGH PRESSURE TURBINE ROTOR BLADE

During the power plant start and stop cycles or load changes, the high pressure turbine blade is exposed to variations in stress and gas temperature levels. The stress level is a function of blade rotational speed, therefore single and multi-shaft gas turbine engines will have different blade stress profiles at part-load. The gas temperature on the other hand is a function of the plant load, which depending on the level will exhibit different mechanical properties.

Figure 3 shows simulated results of stress levels at a notched root of high pressure turbine blade against the mechanical properties of the alloy (Nimonic alloy 115), at part-load operation for single and multi-shaft engine. The figure also shows variations in properties depending on whether the load is reduced by modulating fuel flow, or first closing VIGVs followed by fuel flow reduction.

According to Figure 3, the centrifugal stress at the notch of the blade exceeds the yield stress of the material at all load ranges for single and multi shaft engine. Therefore, plastic deformation will occur locally at the stress concentration region leading to un-recoverable deformation.

The single shaft engine operates at constant rotational speed as required by electrical generator to maintain grid frequency of 50Hz in Europe and 60Hz in Americas. This leads to a usual 3,000 rpm in Europe; therefore, the stress level remains unchanged with only TET and alloy mechanical properties changing at part-load as function of temperature.

The multi-shaft engine contains free power turbine linked to electrical generator and a disconnected gas generator with varying rotational speed at part-load operation giving rise to reduced stress level and changing alloy mechanical properties at part-load.

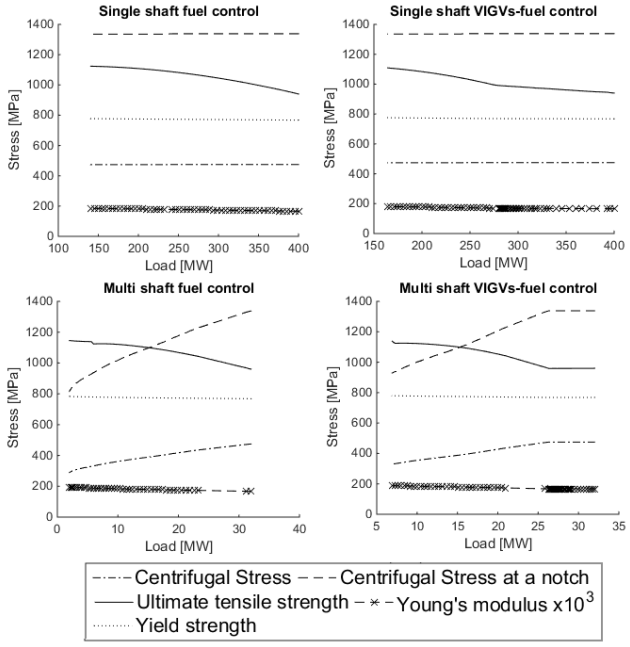

Figure 3 Simulated results of centrifugal stress level in high pressure turbine blade for single and multi-shaft gas turbine against mechanical properties of NIMONIC 115 alloy.

If the local stress level at particular engine part-load operation does not exceed yield strength limit of the alloy, only elastic strain deformation, ε^e, will occur. The loading and unloading under this condition is reversible and the local deformation will return to original shape once the load is removed as shown in Figure 4a, and according to Equation 3. Since the Young's modulus in Figure 3 increases with load reduction, the amount of elastic strain deformation will decrease with load reduction.

Figure 4b shows that the load level is sufficiently large at point A for the local stress to exceed yield strength limit of the material. Therefore, the Neuber's rule, the top of Equation 6, is applied to determine plastic strains and convert an elastically determined stress into actual stress level lying on the material's stress-strain curve. As the result, additionally to elastic deformation, the irreversible plastic deformation will also occur locally according to Equation 4. When the load is removed the local region of stress concentration in the blade will be subject to compressive forces, point C, because irreversible plastic deformation will exert pressure on the surrounding material, which intends to return to its original shape. If the cycle is then repeated up to the same load level, point A or point B after applying Neuber's rule, the already induced plastic deformation will remain, and only local elastic deformation will take place in the material.

According to Figure 4c, if the stress level is sufficiently high, approximately $> 2\sigma_{ys}$, Massing's hypothesis states that the unloading process will follow the Hysteresis stress-strain curve according to Equation 5.

Equation 3

$$\varepsilon^e = \frac{\sigma}{E}$$

Equation 4

$$\varepsilon^p = \left(\frac{\sigma}{K}\right)^{1/n}$$

Equation 5

$$\Delta\varepsilon = \frac{\Delta\sigma}{E} + 2\left(\frac{\Delta\sigma}{2K}\right)^{1/n}$$

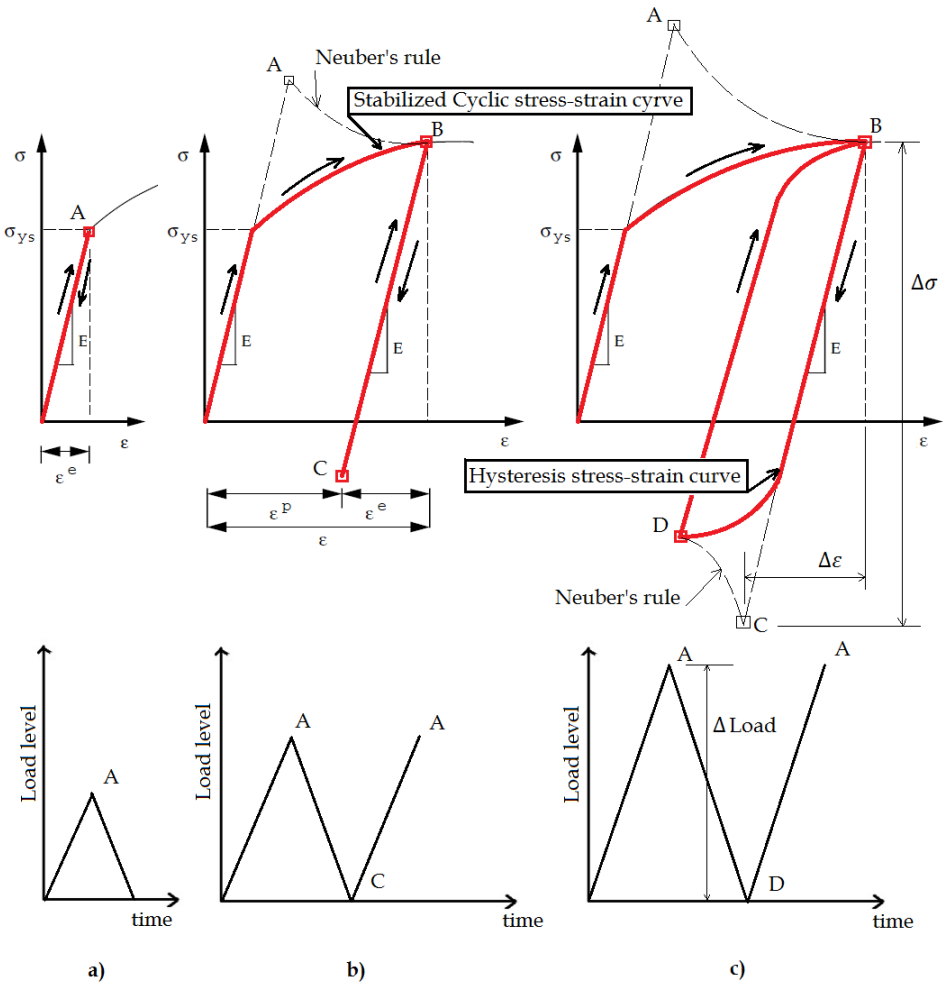

Figure 4 Stress-strain diagram for various load change scenarios.

Therefore, by solving the set of equations in Equation 6, the actual stress and strain levels at local high stress region are obtained at each plant load level.

Equation 6

$$\begin{cases} \dfrac{(K_t\sigma_A)^2}{E} = \sigma_A\varepsilon_A = \sigma_B\varepsilon_B \\ \varepsilon_B = \varepsilon^e{}_B + \varepsilon^p{}_B = \dfrac{\sigma_B}{E} + \left(\dfrac{\sigma_B}{K}\right)^{1/n} \end{cases}$$

During the unloading however, the local coordinate system is used with datum at point B according to Equation 7. Where $\Delta\sigma$ and $\Delta\varepsilon$ represent the actual change in stress and strain level induced by reducing the plant load level, $\Delta Load$.

Equation 7

$$\begin{cases} \sigma_C = \sigma_B - \Delta\sigma \\ \varepsilon_C = \varepsilon_B - \Delta\varepsilon \end{cases}$$

The unloading process, point B-D will follow the Massing curve described by Equation 5. The Neuber's rule is used to convert the stress and strain levels at point C to actual levels at point D. By solving the set of two equations in Equation 8, actual stress and strain levels are obtained at point D as the result of changing plant load level.

Equation 8

$$\begin{cases} \dfrac{(K_t\Delta\sigma)^2}{E} = (\sigma_B - \Delta\sigma)(\varepsilon_B - \Delta\varepsilon) = \sigma_D\varepsilon_D \\ (\varepsilon_B - \varepsilon_D) = \dfrac{(\sigma_B - \sigma_D)}{E} + 2\left(\dfrac{(\sigma_B - \sigma_D)}{2K}\right)^{1/n} \end{cases}$$

Figure 5 and Figure 6 shows simulated results of load cycling for single and multi-shaft engine plotted on stress-strain diagram. The contour lines show load level in MW, the dotted line represents Hysteresis curve, and each dot corresponds to a stress and strain value at a given engine load.

According to Figure 5 for a single shaft engine, the unchanged shaft rotational speed is reflected by unchanged stress value at point A at all levels from 400 MW to 150 MW. The actual stress and strain values at point B have different values of stress due to the fact that mechanical properties of the blade alloy, here Modulus of Elasticity, vary as function of gas temperature according to Figure 3. During the unloading, because the shaft speed remains constant, the $\Delta Load$ has no effect on the change in σ_D and ε_D. For example, according to the figure reducing load from 400 MW to 300 MW and reducing from 400 MW to 150 MW will induce the same compressive stress of approximately -400 MPa and strain of approximately 0.00375.

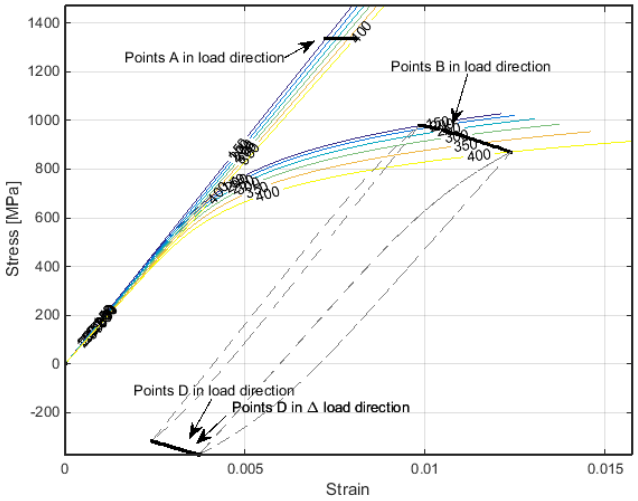

Figure 5 Stress-strain diagram representation of thermal cycling in a high pressure turbine rotor blade at various load levels for single shaft engine.

Figure 6, on the other hand, shows modelled loading and unloading stress-strain profiles for multi shaft engine. Since the gas generator is not physically coupled with the free-power turbine, the load reduction results in changes in engine rotational speed. Therefore, stress varies at point A across the load range from 32 MW to 8 MW, as well as the corresponding actual stress and strain at point B. The contour plot at point D shows the nearly vertical lines, which represent the engine load level in MW, and nearly horizontal lines, which represent the change in load $\Delta Load$ in MW. For example, according to the figure, reducing engine load level from 22 MW to 16 MW will result in stress level change approximately from 900 Mpa in tension at point B to -200 MPa in compression at point D and strain level reduction from approximately 0.0095 to 0.003, accordingly.

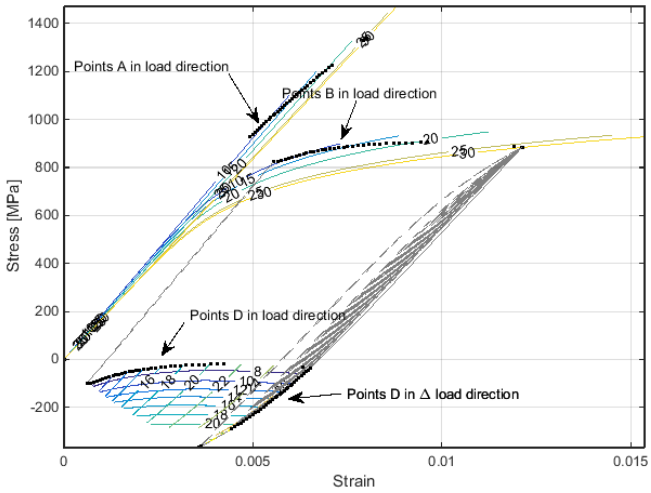

Figure 6 Stress-strain diagram representation of thermal cycling in a high pressure turbine rotor blade at various load levels for multi-shaft engine.

The prediction of life consumption due to low cycle fatigue has been modelled by Marrow, with consistent validation against observations (Bannantine, Comer, & Handrock, 1990). According to Equation 9, knowing the $\Delta\varepsilon$ and σ_m terms, the number of cycles to failure, N_f, is calculated. The cumulative damage is calculated with Equation 10, such that if $D > 1$, the failure will occur.

Equation 9

$$\frac{\Delta\varepsilon}{2} = \frac{\sigma_f' - \sigma_m}{E}\left(2N_f\right)^b + \varepsilon_f'\left(2N_f\right)^c$$

Equation 10

$$Damage = \sum \frac{1}{N_f}$$

CREEP FAILURE OF HIGH PRESSURE TURBINE BLADE

The strength of a turbine blade alloy reduces with increase in gas temperature. At high temperatures and sufficiently long exposure time, the alloy experiences greater mobility of dislocations and an increase in the equilibrium concentration of vacancies. Based on observations, it has been accepted that the effect of creep deformation becomes noticeable when temperature is greater than approximately 40% of the material melting point. Since gas turbine engines operate at high temperatures, this limit is often exceeded giving raise to significant creep life consumption. If high pressure turbine blade is exposed to high stress and temperature for prolonged periods of time, the local stress concentration region will begin to deform known as primary creep. The strain rate then slows down and becomes nearly constant known as secondary or steady-state creep. At some point in time the strain will continue increasing exponentially in the tertiary creep leading to fracture.

The creep fracture can be predicted using a correlative approach. The Larson-Miller parameter is the most popular parametric method due to its high accuracy in predicting failure (Laskaridis, 2013; Eshati, Abdul Ghafir, Laskaridis, & Li, 2010). This parametric expression is calculated using Equation 11.

Equation 11

$$LMP = \frac{T}{1000}\left(\log_{10} t_f + C\right)$$

The constant C is usually taken as 20 for industrial gas turbine engines. The Larson-Miller parameter, LMP, is obtained from alloy experimental curves as function of stress level. Assuming the blade alloy to be NIMONIC 115, which is a common nickel-based alloy used to manufacture high pressure turbine blades, the LMP is calculated with Equation 12 as function of stress level (Isaiah, et al., 2015; Nimonic alloy 115).

Equation 12

$$\begin{cases} LMP = 3.2e^{-5}\sigma^2 - 2.74e^{-2}\sigma + 30.47, & \sigma \le 250MPa \\ LMP = 1.0e^{-5}\sigma^2 - 1.65e^{-2}\sigma + 29.13, & \sigma > 250MPa \end{cases}$$

The cumulative fraction of creep life consumed is calculated by applying Miner's law for linear damage with Equation 13.

Equation 13

$$Creep\ life\ consumed = \sum \frac{t}{t_f}$$

ENGINE LIFE CONSUMPTION MAPS

Figure 7 shows simulated results of fatigue life consumption for a single shaft engine, whereby load is reduced by modulating fuel flow only. Because the rotational speed remains unchanged at all load levels ($\Delta Load$ has no effect on the change in σ_D and ε_D as discussed in preceding paragraphs), the life consumption contour lines are nearly vertical. According to the figure, a load reduction from 400 MW to 300 MW and reduction from 400 MW to 150 MW will consume the same 0.045% of the low cycle fatigue life. If the engine is cycled again the life consumption will be 0.045% + 0.045% = 0.09% according to Equation 10.

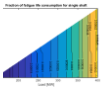

Figure 7 Fatigue life consumption map for high pressure turbine rotor blade in single shaft engine. Load reduction by reducing fuel flow.

Figure 8 shows simulated results of fatigue life consumption for a multi shaft gas turbine engine. The load reduction strategy here is closing VIGVs followed by reduction in fuel flow.

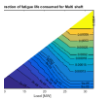

Figure 8 Fatigue life consumption map for high pressure turbine rotor blade in multi-shaft engine. Load reduction by closing VIGVs followed by reduction in fuel flow.

Figure 9 shows simulated results of creep life consumption for a single shaft gas turbine engine. According to the figure, if engine is operated at 400 MW for 400 minutes, approximately 0.2% of life will be consumed due to creep deformations at the root of the high pressure turbine blade. The life consumption is accumulated linearly; therefore, if engine is next operated at 350 MW for 400 minutes, the cumulative life consumed will be 0.2%+0.02%=0.22%.

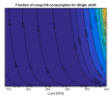

Figure 9 Creep life consumption map for high pressure turbine rotor blade in single shaft engine. Load reduction by reducing fuel flow.

Simulated results of creep life consumption for multi-shaft gas turbine engine are shown in Figure 10. According to the figure, if the engine is operated at 30 MW for 400 minutes, the creep life consumed will be 0.1%. If the load of the engine is then reduced to 20 MW and remained for 400 minutes, the creep life consumed will be 0.1%+0.02%=0.12%.

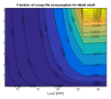

Figure 10 Creep life consumption map for high pressure turbine rotor blade in multi-shaft engine. Load reduction by closing VIGVs followed by reduction in fuel flow.

The life consumption maps can provide means to quickly assess how much life is to be consumed if the plant load is changed for a specific time period, e.g. in the balancing market. The results can be used to further analyse by how much closer will the maintenance schedule shift, and by how much will the maintenance cost increase. Finally, an informed decision can be made whether a particular contract for a load change in the balancing market is profitable enough.

DEVELOPMENT OF GAS TURBINE OPERATIONAL FLEXIBILITY MAP

The operational flexibility of a gas turbine engine is a measure of how quickly it can change load. Since higher operational flexibility makes the power plant more competitive, there is a need for a simple and robust flexibility map to assess economic trade-offs and load change strategies.

Usually gas turbine performance is evaluated by calculating or simulating a large number of parameters and corresponding component characteristics. The complexity of the analysis increases even further if one wishes to evaluate performance trade-offs at engine part-load operating conditions. At each load level, basic engine performance characteristics are dependent on ambient conditions, physical properties of the working fluid, and the load reduction strategy. Parametric studies of these variables and their effect on part-load engine performance have been discussed widely in recent years (Haglind, 2010; Kim, Kim, Sohn, & Ro, 2003; Kim T. S., 2004). It is clear that full variation of engine performance quantities affecting flexible operation involves complex and excessive number of calculations and visual

representations, which can make a concise presentation of the results unachievable.

A Buckingham pi theorem allows analysing complex systems and combining variables into smaller dimensionless groups. According to the theorem, n number of variables can be reduced to n-3 dimensionless groups due to presence of three fundamental units – mass, length and time. The form of the dimensionless groups is highly dependent on the selection of three repeating variables, which appear in all pi terms and should contain all three fundamental units. Upon careful analysis I concluded that these should represent variables which cannot be controlled or changed, such as 1) compressor characteristic diameter representing the engine size, 2) ambient temperature, and 3) ambient pressure.

Assuming that the working fluid behaves as an ideal gas, the temperature can be represented as $RT = \frac{P}{\rho}$ with fundamental dimensions of $[L^2T^{-2}]$. Therefore, presence of the gas constant, R, allows for the operational flexibility map to be analysed for various kinds of working fluids. The rest of the performance parameters and their respected fundamental units are listed in Table 2.

Table 2 Dimensions of main performance parameters

Variable	Fundamental dimensions	Comments
$\boldsymbol{D}$	[L]	Repeating variable. Compressor characteristic diameter
$\boldsymbol{(RT)_{amb}}$	$[L^2T^{-2}]$	Repeating variable. Ambient temperature
$\boldsymbol{P_{amb}}$	$[ML^2T^{-2}]$	Repeating variable. Ambient pressure
$\boldsymbol{N}$	$[T^{-1}]$	Engine rotational speed
$\boldsymbol{\dot{m}_{ff}}$	$[MT^{-1}]$	Fuel mass flow
$\boldsymbol{VIGV}$	[]	Angle of VIGVs
$\boldsymbol{PO_{GT}}$	[MT]	Gas turbine power output
$\boldsymbol{RTET}$	$[L^2T^{-2}]$	Turbine entry temperature
$\boldsymbol{RT_{exhaust}}$	$[L^2T^{-2}]$	Turbine entry temperature
$\boldsymbol{\dot{m}_{GT,in}}$	$[MT^{-1}]$	Inlet mass flow
$\boldsymbol{ETA_{GT}}$	[]	Gas turbine thermal efficiency

An important decision to a power plant operator is on a load change strategy. For a given gas turbine technology, a chosen strategy determines a degree improvement or deterioration in flexibility which can make a power plant more or less economically attractive. Therefore, abscissa and ordinate for every point on the map should represent a general load change dimensionless group. The load of a gas turbine engine can be changed using various techniques, each of which results in a certain degree of economic consequences. The two main techniques to change the load are to control variable area or fuel flow. The modulation in VIGVs angle at the inlet to the low pressure compressor affects the rate of air mass flow into the compressor. Change in engine inlet mass flow has a large effect on power output. Apart from the preferred method of varying VIGVs angle, the inlet air mass flow and resulting load level can also be changed by preheating inlet air, or extracting bleed from the compressor. Therefore, inlet air mass flow on the x-axis is an important parameter for any load reduction strategy. On the second strategy, modulation in fuel flow results in changes in temperature at the inlet to the turbine, which affects gas energy content and expansion capacity across the turbine. Generally, first stage turbine rotor blades are very sensitive to a variation in flow path temperature. Therefore the turbine entry temperature on the y-axis is one of the main parameters that must be closely monitored while changing engine load. As the result, the first two dimensionless groups forming x and y axis on the map are: the non-dimensional inlet air mass flow, π_1, and non-dimensional turbine entry temperature, π_2. The calculations for the first non-dimensional group are shown below, and the methodology is then repeated to obtain the rest of the groups.

The first three terms in Equation 14 are repeating variables, and the last term represents inlet air mass flow. Equating fundamental units

Equation 14

$$D^a (RT)_{amb}{}^b P_{amb}{}^c \dot{m}_{GT,in}{}^d = [\mathrm{L}]^a[\mathrm{L}^2\mathrm{T}^{-2}]^b[\mathrm{ML}^2\mathrm{T}^{-2}]^c[\mathrm{MT}^{-1}]^d$$

This gives the following set of linear equations

$$\begin{cases} c + d = 0, & for\ M \\ -2b - 2c - d = 0, & for\ T \\ a + 2b + 2c = 0, & for\ L \end{cases}$$

Writing all coefficients in terms of d

$$\begin{cases} c = -d, & for\ M \\ b = 0.5d, & for\ T \\ a = d, & for\ L \end{cases}$$

Plugging coefficients into original equation, gives the first non-dimensional mass flow group

$$\pi_1 = D^d (RT)_{amb}{}^{0.5d} P_{amb}{}^{-d} \dot{m}_{GT,in}{}^d$$

Equation 15

$$\pi_1 = \frac{D\dot{m}_{GT,in}\sqrt{(RT)_{amb}}}{P_{amb}} = \frac{\dot{m}_{GT,in}\sqrt{T_{amb}}}{P_{amb}}$$

Similarly the non-dimensional TET

Equation 16

$$\pi_2 = \frac{RTET}{(RT)_{amb}} = \frac{TET}{T_{amb}}$$

Non-dimensional gas turbine power

Equation 17

$$\pi_3 = \frac{[(RT)_{amb}]^{3/2} PO_{GT}}{DP_{amb}} = \frac{{T_{amb}}^{3/2} PO_{GT}}{P_{amb}}$$

Non-dimensional angle of VIGVs

Equation 18

$$\pi_4 = VIGV$$

Non-dimensional gas turbine efficiency

Equation 19

$$\pi_5 = ETA_{GT}$$

And non-dimensional gas turbine exhausts temperature

Equation 20

$$\pi_6 = \frac{T_{exh}}{T_{amb}}$$

Having worked out all of the PI terms, the relation of any selected non-dimensional group can be expressed as function of the others. For example,

$$\pi_3 = f(\pi_1, \pi_2, \pi_4, \pi_5)$$

Or

$$\frac{[(RT)_{amb}]^{3/2} PO_{GT}}{DP_{amb}} = f\left(\frac{D\dot{m}_{GT,in}\sqrt{(RT)_{amb}}}{P_{amb}}, \frac{RTET}{(RT)_{amb}}, VIGV, ETA_{GT}\right)$$

Rearranging the equation further

Equation 21

$$PO_{GT} = \left(\frac{D}{R^{3/2}}\right)\left(\frac{P_{amb}}{{T_{amb}}^{3/2}}\right) f\left(\frac{D\dot{m}_{GT,in}\sqrt{(RT)_{amb}}}{P_{amb}}, \frac{RTET}{(RT)_{amb}}, VIGV, ETA_{GT}\right)$$

GAS TURBINE OPERATIONAL MAP

Figure 11 shows calculated lines of constant non-dimensional power output as function of non-dimensional inlet mass flow and non-dimensional TET for a single shaft gas turbine engine. Because of the assumption that the turbine remains choked at part-load, the TET must increase to accommodate reduction in inlet mass flow in order for the engine to remain at constant power. Therefore, the constant power output lines have negative slopes.

Performance simulation results show that the fuel flow depends linearly on the engine power output. Therefore, non-dimensional power output lines can be replaced with non-dimensional fuel flow, as calculated and shown in Figure 12. The thermal efficiency is already a non-dimensional group by definition, of which constant contour lines are calculated and shown in Figure 13.

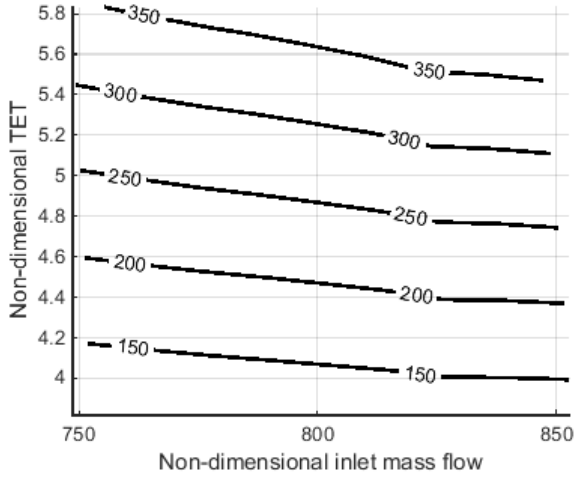

Figure 11 Gas turbine operational flexibility map with constant non-dimensional power output lines for single shaft engine.

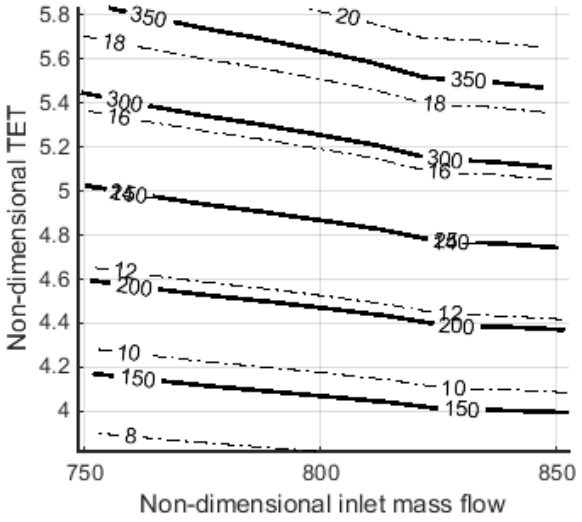

Figure 12 Gas turbine operational flexibility map with additional constant non-dimensional fuel flow dotted lines for single shaft engine.

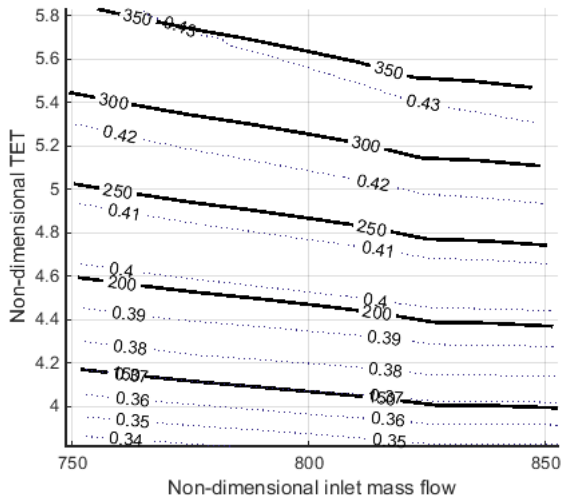

Figure 13 Gas turbine operational flexibility map with additional constant non-dimensional thermal efficiency lines for single shaft engine.

Examining operational flexibility map in Figure 11 clearly reveals that engine power can be varied at constant non-dimensional TET, constant non-dimensional inlet mass flow, or perhaps any other combination of these two non-dimensional groups. The most common load change strategies are modulating VIGVs angle at constant Texh in CCPP application, modulating VIGVs at constant TET in simple cycle application, or modulating fuel flow (Dechamps, 2016).

Load change by modulating Variable Inlet Guide Vane angle

Variable Inlet Guide Vanes (VIGVs) are variable geometry stator blades fitted at the first few stages of a low pressure compressor. By closing VIGVs, the engine swallowing capacity is effectively reduced, which by definition reduces the amount of power output. Most of the large industrial gas turbine engines have 1-4 rows of VIGVs, which allow for up to 30% airflow reduction and corresponding 50% power reduction (Kim, Kim, Sohn, & Ro, 2003).

The angle of VIGVs is already a non-dimensional group by definition, of which constant lines are calculated and shown in Figure 14 together with constant non-dimensional power. The angle is referenced from the design position of the variable geometry blades at 0°. At each constant VIGVs line, the non-dimensional inlet mass flow increases slightly with load reduction. This is due to the assumption that the turbine remains choked at part-load; therefore, reduction in TET is compensated with a small increase in inlet air mass flow.

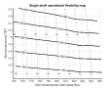

Figure 14 Gas turbine operational flexibility map with additional constant dotted lines of VIGVs angle for single shaft engine.

Figure 15 shows modelled constant non-dimensional exhaust temperature lines together with non-dimensional power and efficiency. The exhaust temperature is an important parameter if a bottoming cycle is used to extract energy from the gas turbine exhaust to improve overall combined cycle efficiency, and power output. It is a common practice to install shell-and-tube type heat exchanger in the exhaust duct to extract energy from the exhaust flow. In this case, the plant operator must monitor the exhaust temperature not to exceed thermal limits of the heat exchanger tube materials; otherwise the component may fail incurring extensive costs during plant shut down for maintenance. As the load of an engine is reduced, the exhaust temperature is kept nearly constant by modulating fuel flow. A line is indicated in the figure illustrating a load reduction from approximately 310 MW to 270 MW at constant exhaust temperature by closing VIGVs angle from 0° to 7°. The non-dimensional TET is reduced from 5.2 to 5.15, resulting in life reduction due to thermal cycling. The thermal efficiency is reduced from approximately 42.6% to 41.6%. In a real engine, however, VIGVs can be closed much further up to 40°, which implies much greater reduction in TET and consequent greater life consumption.

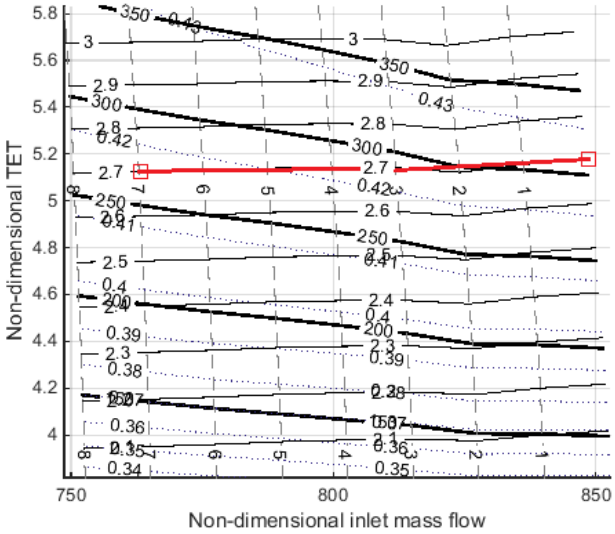

Figure 15 Gas turbine operational flexibility map. Shown load reduction line by closing VIGVs at constant exhaust temperature.

The second common strategy for load reduction is to modulate VIGVs angle at constant TET. For a simple cycle this load reduction strategy results in much better part-load efficiency as compared to VIGVs modulation at constant Texh because according to Figure 13 the constant efficiency lines are degrading much slower at constant TET lines. According to Figure 16, not only the efficiency is improved but also thermal cycling in the hot-path turbine region is removed by keeping TET constant. For example, load reduction from 310 MW to 270 MW by reducing VIGVs angle from 0° to 8° will see constant non-dimensional TET at 5.2 and thermal efficiency reduction from approximately 42.6% to 41.7%. Therefore, there is a slight improvement in thermal efficiency comparing to reducing load by closing VIGVs at constant exhaust temperature. This load reduction strategy improves gas turbine component life at a cost of increasing exhaust gas temperature, which could lead to heat recovery steam generator failure.

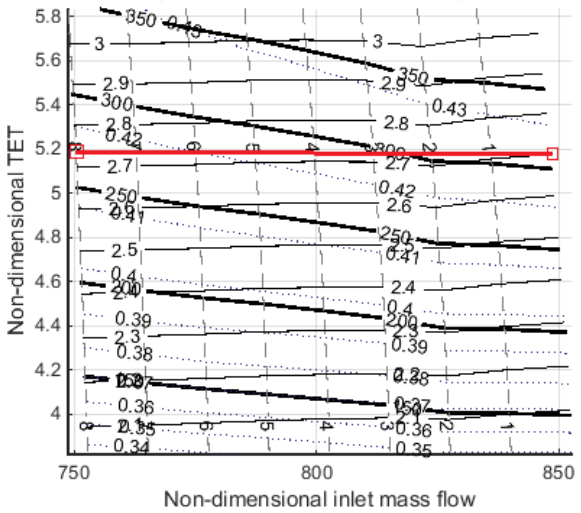

Figure 16 Gas turbine operational flexibility map. Shown load reduction line by closing VIGVs at constant TET.

Load change by reducing fuel flow rate

The operation of an engine with power reduced by modulating fuel flow at constant VIGVs angle is calculated and shown on engine operational flexibility map in Figure 17. The load is reduced from 310 MW to 250 MW at 1° VIGVs angle. However, this requires a large thermal cycling in the hot-path components and much more rapid reduction in thermal efficiency.

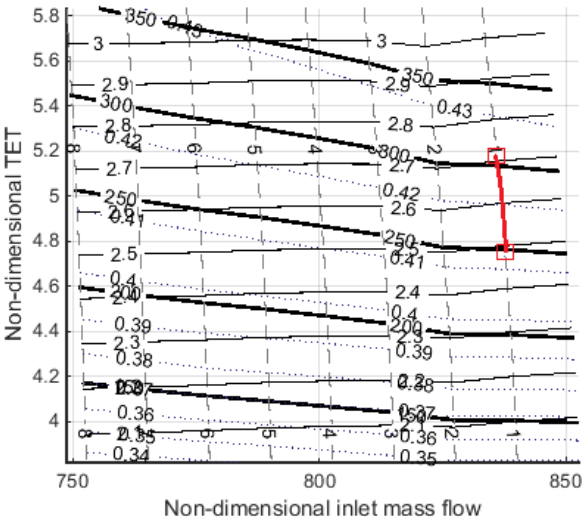

Figure 17 Gas turbine operational flexibility map. Shown load reduction line by fuel flow modulation at constant VIGVs.

New load change strategy for improved flexibility

It appears clearly in Figure 11 that power reduction at constant non-dimensional inlet mass flow takes place more rapidly than at constant non-dimensional TET. The engine appears to be more responsive to a fuel flow modulation rather than changing inlet air mass flow. Therefore, there

must be a path with a combination of non-dimensional TET and non-dimensional inlet air mass flow that will allow for the most responsive load reduction. This is in the normal direction to the constant non-dimensional power lines. For a given engine, keeping all physical parameters unchanged, the highest flexibility path of changing load from for example 310 MW to 250 MW is shown in Figure 18. This can be done by a major modulation in non-dimensional TET from 5.2 to 4.8, e.g. by altering fuel flow rate, and with a minor change in non-dimensional inlet mass flow, e.g. by pre-heating inlet air to reduce density, inlet air bleed extraction, or variable geometry by closing VIGVs by approximately 0.2°.

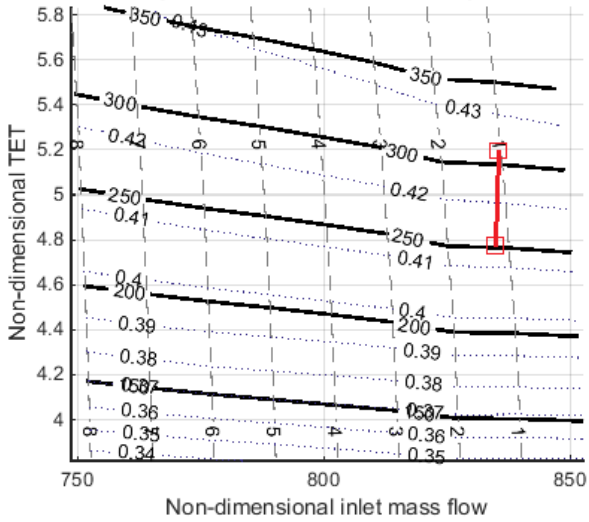

Figure 18 Gas turbine operational flexibility map. Shown load reduction line by a combination of non-dimensional TET and non-dimensional inlet mass flow modulation to achieve higher operational flexibility.

This strategy however, comes with the following trade-offs

- Hot gas path components are very sensitive to a change in gas temperature. Varying TET affects component life due to thermal cycling, which could be avoided by reducing load at constant non-dimensional TET however, at lower flexibility.
- As illustrated in Figure 13, the gas turbine efficiency is degrading more rapidly at constant non-dimensional inlet mass flow than constant non-dimensional TET.

CONCLUSIONS

The work discussed in this paper is an attempt to provide more robust and simpler method to assess gas turbine flexible operation and life consumption in a high pressure turbine rotor blade, as required by changing market conditions. The operational flexibility map exposes new and potentially economically attractive load reduction strategies to maximise the flexibility, and exposes relevant trade-offs in performance.

Some of the prospects for use include:

- The operational flexibility map allows for a quick assessment of the best route to change load of an engine,
- Plant operator may shade areas on the map to visualise regions in which power plant should not operate. For example region of high exhaust temperature in consideration of HRSG failure, region of high TET in consideration of turbine failure, or region of low mass flow in consideration of compressor stalling,
- It could be used by traders and financial advisers to make informed decision weather a given power plant can secure enough profit in the balancing market,
- It could be used to understand hidden costs associated with a decision whether to accept contract in balancing market. These costs could include: increased maintenance costs, or increased fuel costs,
- It could be used to aid internal plant performance modelling,
- It could be used by plant operator to quickly perform preliminary study of any plant upgrades, and assess impact on gas turbine flexible performance,

NOMENCLATURE

ρ	–	Working fluid density
ω	–	Shaft rotational speed
R_t	–	Blade tip radius
R_r	–	Blade root radius
T_{blade}	–	Blade surface temperature
TET	–	Turbine entry temperature
CE	–	Cooling effectiveness
$T_{cooling}$	–	Cooling flow temperature
T_{exh}	–	Exhaust temperature
σ_{ys}	–	Yield stress of a material
ε	–	Strain
σ	–	Stress
E	–	Young's modulus of elasticity
$\Delta\varepsilon$	–	Change in strain
$\Delta\sigma$	–	Change in stress
K	–	Cyclic strength coefficient
n	–	Cyclic strain hardening exponent
K_t	–	Stress concentration factor
LMP	–	Larson-Miller parameter
T	–	Temperature
t_f	–	Time to failure
C	–	Creep constant
t	–	Creep exposure time
$\sigma_f^{'}$	–	Fatigue strength coefficient
σ_m	–	Mean stress
$\varepsilon_f^{'}$	–	Fatigue ductility coefficient
N_f	–	Number of cycles to failure
b	–	Fatigue ductility exponent
c	–	Fatigue strength exponent
D	–	Characteristic engine diameter

T_{amb}	–	Ambient temperature
P_{amb}	–	Ambient pressure
N	–	Engine rotational speed
$\dot{m}_{ff}$	–	Fuel mass flow rate
$VIGV$	–	Variable Inlet Guide Vanes
PO_{GT}	–	Power output of gas turbine
$\dot{m}_{GT,in}$	–	Inlet air mass flow rate
ETA_{GT}	–	Gas turbine thermal efficiency
R	–	Gas constant

ACKNOWLEDGMENTS

The work presented in this paper is an independent research undertaken in partial fulfillment towards a PhD degree and funded by the Flex-E Plant Project, UK.

REFERENCES

Alvarez, T. (2016). *Combined Cycle Power Plant Short Course*. Cranfield: Cranfield University.

Balancing Mechanism Reporting System (BMRS). (n.d.). Retrieved August 08, 2016, from http://www.bmreports.com/

Bannantine, J. A., Comer, J. J., & Handrock, J. L. (1990). *Fundamentals of Metal Fatigue Analysis*. New Jersey: Prentice-Hall.

Dechamps, P. (2016). *Combined Cycle Power Plant Short Course*. Cranfield: Cranfield University.

Eshati, S., Abdul Ghafir, M. F., Laskaridis, P., & Li, Y. G. (2010). IMPACT OF OPERATING CONDITIONS AND DESIGN PARAMETERS ON GAS TURBINE. *ASME Turbo Expo 2010: Power for Land, Sea and Air*. Glasgow: ASME.

Haglind, F. (2010). Variable geometry gas turbines for improving the part-load performance of marine combined cycles – Gas turbine performance. *Energy, 35*(2), 562–570.

Isaiah, T., Dabbashi, S., Bosak, D., Sampath, S., Di-Lorenzo, G., & Pilidis, P. (2015). Life Analysis of Industrial Gas Turbines Used As a Back-Up to Renewable Energy Sources. *The Fourth International Conference on Through-life Engineering Services*. ELSEVIER.

Kim, J. H., Kim, T. S., Sohn, J. L., & Ro, S. T. (2003). Comparative Analysis of Off-Design Performance Characteristics of Single and Two-Shaft Industrial Gas Turbines. *J. Eng. Gas Turbines Power, 125*(4), 954.

Kim, T. S. (2004). Comparative analysis on the part load performance of combined cycle plants considering design performance and power control strategy. *Energy, 29*(1), 71–85.

Laskaridis, P. (2013). *Mechanical Design of Turbomachinery*. Cranfield: Cranfield University.

Nimonic alloy 115. (n.d.). Retrieved from specialmetals.com